Active sensing during a visual perceptual decision-making task

Naureen Ghani[1,†] and the International Brain Laboratory

20 November 2025

[1]Sainsbury Wellcome Centre for Neural Circuits and Behaviour, University College London, London, UK

[†]Correspondence to naureen.ghani.18@alumni.ucl.ac.uk

Abstract

From the Welsh tidy mouse to the New York City pizza rat, movement reveals rodent intelligence. Here, we show that some head-fixed mice develop an active sensing strategy in a visual perceptual decision-making task (**The International Brain Laboratory, 2021**). Akin to humans shaking a computer mouse to find the cursor on a screen, some mice wiggle a wheel that controls the movement of a visual stimulus during low-contrast trials. When mice wiggle, low visual stimulus contrast accuracy increases (weighted linear regression, $R^2 = 0.949, F(1,6) = 111.4, p = 4.26 \times 10^{-5}, N = 8$ group medians from 213 mice). Moreover, these wiggles move the visual stimulus at a temporal frequency (11.52 ± 2.45 Hz) close to the frequency that maximizes visual contrast sensitivity in rodents (**Umino et al, 2018**). These findings suggest that some mice wiggle the wheel to boost the salience of low visual contrast stimuli.

Highlights

- There is a strong, positive relationship between wheel motion energy and the low visual stimulus contrast accuracy across 213 mice.
- Mouse wiggles move the visual stimulus at a median temporal frequency that closely matches the maximum temporal contrast sensitivity (**Umino et al, 2018**).
- Mouse wiggles are not explained by arousal. The mean pupil diameter is comparable between wiggles and non-wiggles.
- Decoding visual stimulus identity from neural activity improves with longer wiggles in midbrain and thalamic regions, including the superior colliculus.

1 Introduction

Active sensing is the use of movement to enhance sensory perception. It is well-studied in freely moving worms (Kato et al, 2015), flies (Fenk et al, 2022; Wang et al, 2022), and rats (Kurnikova et al, 2017; Liao and Kleinfeld, 2023). Sensing actions often involve moving the stimulus into a region of high acuity (Zhaoping, 2019). For example, visual active sensing in humans and monkeys relies on the fovea, which is the high-acuity region of the retina. Humans use eye fixations to improve discrimination of high spatial frequency stimuli (Rucci et al, 2007) and adapt micro-saccades to improve visual acuity (Intoy and Rucci, 2020; Zhao et al, 2023). Similarly, head-fixed monkeys use eye saccades to sample a visual scene (Mitchell et al, 2014; Xiao et al, 2024; Singh et al, 2025).

Since rats and mice are non-foveal, active sensing in rodents is often studied in the somatosensory and olfactory systems rather than the visual system. Rats and mice use whisking to locate objects in space (Diamond et al, 2008; Kleinfeld and Deschênes, 2011) and sniffing to sample olfactory information (Wachowiak, 2011; Shusterman et al, 2011). Active sampling of touch and smell in rodents involves coordinated movements of head bobbing, nose twitching, whisking, and breathing (Kurnikova et al, 2017; Liao and Kleinfeld, 2023). These rhythmic head and orofacial movements are controlled by pre-motor oscillator networks in the brainstem (Moore et al, 2013; Takatoh et al, 2022; Kaku et al, 2025).

Active vision in rodents has been primarily studied with freely-moving animals (Skyberg and Niell, 2024). During natural visual behaviors, mice coordinate eye, head, and body movements to detect threats (Yilmaz and Meister, 2013; De Franceschi et al, 2016), capture prey (Hoy et al, 2019), and judge depth (Boone et al, 2021; He et al, 2024). When mice explore an arena with a visual display of spots varying in spatial and temporal frequencies, neurons in primary visual cortex (V1) respond most strongly to gaze shifts (Parker et al, 2023). Similar gaze-shift

responses are observed in the superficial layers of the superior colliculus (sSC), whereas deeper layers (dSC) instead exhibit motor-related activity aligned to head movements (Sharp et al, 2025). This suggests that gaze-shifting head and eye movements follow a dynamic temporal sequence (Skyberg et al, 2022) in neural activity as mice engage in naturalistic active vision.

The interaction of vision and movement in locomotion is well-studied in head-fixed mice. Mouse V1 encodes locomotion (Niell and Stryker, 2010; Keller et al, 2012; Ayaz et al, 2013; Saleem et al, 2013; Stringer et al, 2019) and locomotion enhances neural encoding of visual stimuli in mouse V1 (Dadarlat and Stryker, 2017; Dipoppa et al, 2018). The majority of mouse V1 neurons are modulated by head movements (Meyer et al, 2020) in a luminance-dependent manner (Bouvier et al, 2020; Guitchounts et al, 2020). Mouse eye saccades tend to be coupled to head movements (Parker et al, 2022) and while head-fixed mice do saccade, these movements are likely not predominantly visually driven (King et al, 2023).

Spontaneous, uninstructed movements and arousal influence head-fixed mouse neural activity. When head-fixed mice are allowed to run freely on a spherical treadmill (Dombeck et al, 2007), locomotion increases the neuronal signal-to-noise ratio in V1 (Bennett et al, 2013). Although the relationship between V1 activity and locomotion (associated with high arousal) is monotonically increasing, mice perform a visual detection task best during intermediate levels of arousal (Neske et al, 2019). Both arousal dynamics and uninstructed movements predict mouse performance in visual tasks (Hulsey et al, 2024). As mice become less engaged and perform biased choices, widespread cortical activity variance increases, spontaneous movement stereotypy decreases, and pupil diameter remains stable (Yin and Melin et al, 2025). Together, these findings suggest that there is strong link between uninstructed movements, arousal levels, and neural activity in head-fixed mice performing visual tasks.

Although the neural mechanisms for active vision are not yet fully known in head-fixed mice, this has been well-studied in non-human primates. From spatio-temporally precise retinal input (Sun et al, 2004; Schottdorf and Lee, 2022) to attention-driven eye saccades (Moore et al, 2003), information passes from dorsal cortex to the superior colliculus (Goldberg and Wurtz, 1972; Hafed et al, 2021). While eye movements in mice are different from those in monkeys (Meyer et al, 2020; Giovannetti and Rancz, 2024; Kang et al, 2025), we posit that head-fixed mice physically manipulate a wheel to the same effect.

We propose that head-fixed mice develop an active sensing strategy while performing a visual decision-making task. Our hypothesis is that mice wiggle a wheel that controls the movement of a visual stimulus when sensory information is limited. Wiggling transforms a spatial frequency into a temporal frequency, which boosts the salience of the visual stimulus, as the mouse visual system is particularly sensitive to temporal changes (Gulbinaite et al, 2024).

We test this hypothesis using large-scale data analysis approaches across and within mice. We ask (1) does the low visual stimulus contrast accuracy increase with wiggles? This question is motivated by examples of visual accuracy gains with head-movement jitters (Fulvio et al, 2021) and retinal-image jitters (Palmisano et al, 2009; Watson et al, 2012) in humans. (2) Are wiggles explained by arousal or change-of-mind? This question is motivated by examples of head-fixed mice fidgeting when aroused (Musall et al, 2019) and monkeys reversing movement trajectories with more evidence during decision-making tasks (Kaufman et al, 2015). (3) Are higher speed wiggles more accurate? This question is motivated by studies that demonstrate improvement in psychophysical performance with higher speed visual stimuli in humans (Rolfs et al, 2025) and monkeys (Huang et al, 2024). Motivated by classic examples of active sensing in freely moving rodents such as whisking and sniffing, we used continuous and discrete metrics of wiggles to determine whether head-fixed mice benefit from an active sensing strategy during a visual perceptual decision-making task.

1.1 Mice used a wheel to center a visual stimulus for sugar-water reward.

We analyzed behavioral data from 213 mice that performed a visual perceptual decision-making task while head-fixed (**Figure 1a**). Mice were trained to use a miniature steering wheel that controlled the movement of a visual stimulus (The International Brain Laboratory, 2021). When mice moved the wheel for a total of 8.75 millimeters to center the visual stimulus, they earned sugar-water reward (**Figure 1b**). With a visuo-motor gain of 4 visual degrees per millimeter of wheel movement, this 8.75 mm corresponded to 35 visual degrees of stimulus movement (8.75 mm $\times$ 4 visual degrees/mm = 35 visual degrees).

We used a shaping protocol to gradually train mice to perform the visual decision-making task at increasingly difficult contrast levels. Mice began with trainingChoiceWorld sessions (left and right stimuli were presented with equal probability) containing only 100% and 50% contrast trials. When the proportion correct reached 70%, we consecutively added lower contrast trials: first adding 25% contrast, then adding 12.5% contrast while replacing 50% with 0% contrast trials, and finally adding 6.25% contrast trials. These final sessions with the full range of contrast levels (100%, 25%, 12.5%, 6.25%, and 0%) constituted the late stage trainingChoiceWorld sessions used for analysis.

After learning the visual detection task, mice progressed to biasedChoiceWorld sessions (left and right stimuli were presented with unequal probability) (see Appendix 2 of The International Brain Laboratory et al, 2021 for

details). When neural data was acquired during these biasedChoiceWorld sessions, we refer to them as ephysChoiceWorld sessions.

Our behavioral dataset consisted of three session types: 54.36% biasedChoiceWorld sessions (2761 sessions), 38.94% late stage trainingChoiceWorld sessions (1978 sessions), and 6.70% ephysChoiceWorld sessions (340 sessions).

The probability of a left visual stimulus was manipulated in strictly alternating biased blocks for sets of $20-100$ trials (**Figure 1c**). A session consisted of (1) 90 trials in an unbiased block (50/50) followed by (2) $4-5$ left (80/20) and right (20/80) blocks. The independent variable was visual stimulus contrast, which ranged from high (1.0), intermediate (0.25 and 0.125), low (0.0625), and zero (0.0) (**Figure 1d**). Each trial had a variable quiescent period duration from 0.40 to 0.70 seconds (computed as 0.2 seconds + a duration drawn from an exponential distribution with a mean of 0.35 seconds, min and max of 0.20–0.50 seconds) (**Figure 1e**) (Appendix 2 of The International Brain Laboratory et al, 2021). The inter-trial interval was fixed at 0.5 seconds for correct trials and 2 seconds for error trials.

The reaction time distribution across mice ($3,329,275$ trials) was bimodal, which is how we defined 0.08 seconds as the threshold for a visual stimulus-triggered response (**Figure 1f**). We plotted reaction times between -0.20 and 0.50 seconds, which represents 86.10% of the data. This implies that the proportion of data not shown in **Figure 1f** is 13.90%, where the reaction time exceeded 0.50 seconds. During visual stimulus-triggered trials, the proportion of counterclockwise choices was a function of block (**Figure 1g**). Thus, mouse behavior was biased by blocks.

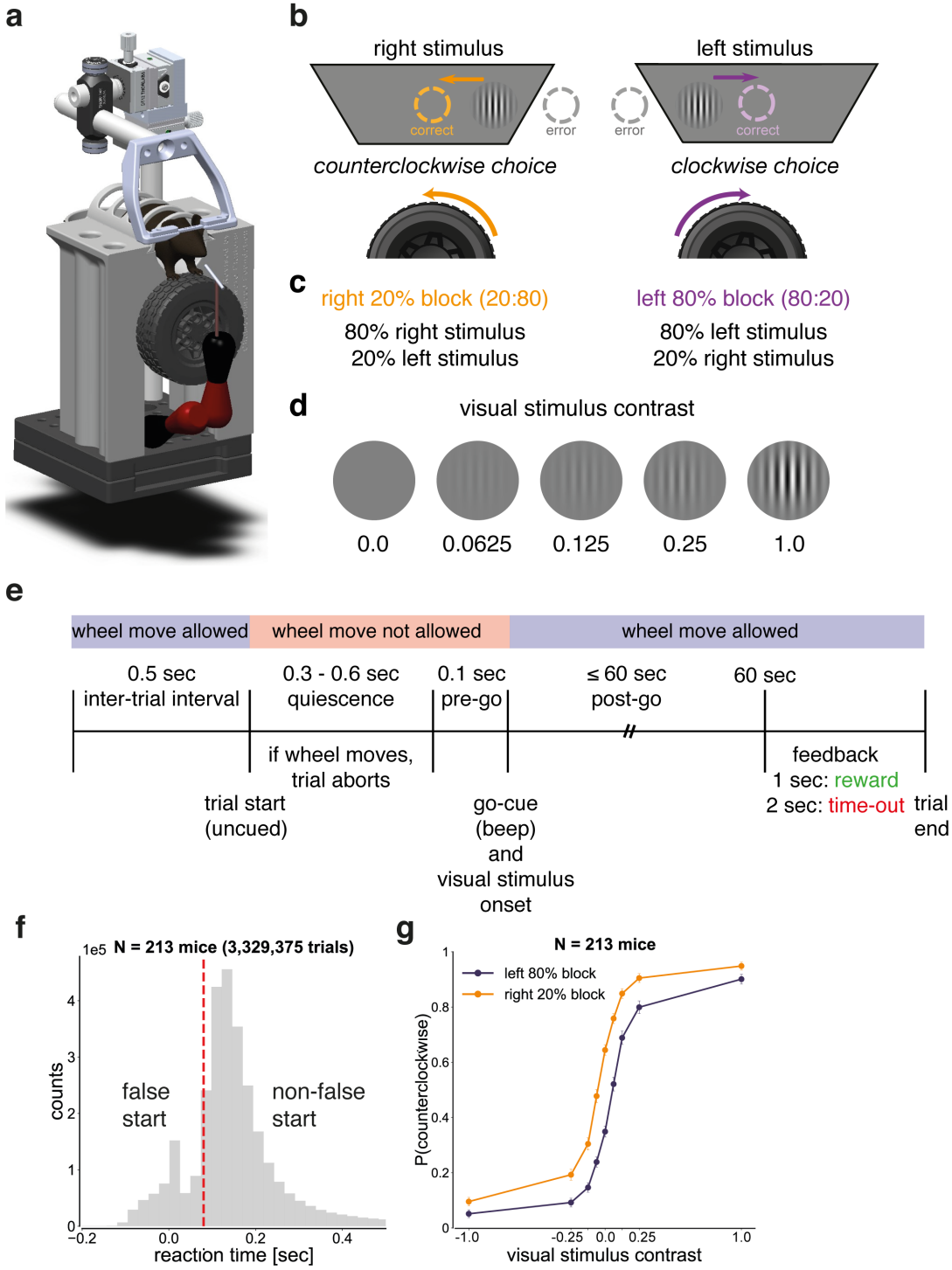

Figure 1: **Mice used a wheel to center a visual stimulus for reward.** **(a)** A head-fixed mouse used a miniature steering wheel (The International Brain Laboratory, 2021) to indicate choice. Schematic by: Florian Rau. **(b)** Mice turned the wheel counterclockwise for a right visual stimulus and clockwise for a left visual stimulus to earn sugar-water reward. Mice received negative feedback (a 2-second time-out with a gray screen) if the visual stimulus fell off the screen. **(c)** The task has a block structure. The **left 80% block** consisted of 80% left visual stimuli and 20% right visual stimuli (**80:20**). The **right 20% block** was the converse and consisted of 80% right visual stimuli and 20% left visual stimuli (**20:80**). **(d)** The independent variable was visual stimulus contrast: $[0.0, 0.0625, 0.125, 0.25, 1.0]$. **(e)** The task has a trial structure with a variable quiescent period duration ($0.4 - 0.7$ seconds) and a free-response period (60 seconds). **(f)** The reaction time distribution inclines at 0.08 seconds across $N = 213$ mice, which is the threshold for non-false starts (indicated by red dashed line). **(g)** The psychometric curves were dependent on visual stimulus contrast (one-way repeated measures ANOVA, **left 80% block:** $F = 982.3, p < 0.001$, **right 20% block:** $F = 1109.7, p < 0.001$) and block (one-way repeated measures ANOVA, $p < 0.05$) in non-false starts. Error bars represent the binomial proportion confidence intervals (CI).

2 Results

2.1 Wiggles are wheel movements with multiple changes in wheel direction.

To determine whether low visual stimulus contrast accuracy depends on wheel movement dynamics, we defined a discrete measure of directional changes. This metric is denoted as k, which quantifies the number of changes in wheel movement direction during a trial.

This was computed from wheel position data interpolated at 1000 Hz, which captured the general motion of the wheel with superimposed rapid directional changes. Directional changes were identified by counting zero crossings in the derivative of the position signal, which were points where the wheel velocity (in degrees per second) changed sign.

The wheel data in each mouse was stratified by k into one of five groups: (1) $k = 0$, (2) $k = 1$, (3) $k = 2$, (4) $k = 3$, and (5) $k \geq 4$.

k value	Movement pattern	Interpretation	Wiggle?
0	single-direction movement	ballistic, confident choice	No
1	one directional change	change-of-mind or near-ballistic	No
≥ 2	multiple directional changes	active sensing, change-of-mind, or disengagement	Yes

Table 1: **Summary of wheel movement dynamics.** k is the number of directional changes.

A trial with $k = 0$ directional changes is defined as a non-wiggle (**Figure 2a**). Such trials are examples of ballistic movements, which are high-velocity, high-acceleration movements done within a short period of time.

A trial with $k = 1$ directional changes is defined as a non-wiggle with one sign reversal (**Figure 2b**). Such trials could represent change-of-mind, which is a revision in the initial choice based on accumulated evidence (**Figure 1b**). An alternative explanation is that $k = 1$ directional changes are near-ballistic movements. To distinguish change-of-mind from near-ballistic, reaction time and wheel amplitude can be used. While near-ballistic movements will have fast reaction times ($0.1 - 0.2$ seconds) and small wheel amplitudes (below 2 degrees), change-of-mind trials will have longer reaction times indicative of deliberation ($0.4 - 0.5$ seconds) and greater wheel amplitudes (upwards of 2 degrees) indicative of evidence accumulation.

A trial with $k \geq 2$ directional changes is defined as a wiggle (**Figure 2c–f**). We considered three possible interpretations of wiggles: (1) active sensing, (2) change-of-mind, and (3) disengagement.

- **Active sensing hypothesis:** Mice wiggle the wheel to enhance perception because it is easier to detect a moving visual stimulus than a static one. In this view, the jitter serves as a strategy for accumulating sensory evidence by dynamically modulating the visual input.
- **Change-of-mind hypothesis:** Mice wiggle the wheel due to uncertainty about the correct decision. In this view, the jitter represents hesitation between the leftward and rightward choices as the mouse re-evaluates its initial decision.
- **Disengagement hypothesis:** Mice wiggle the wheel because they are disengaged from the task. In this view, the jitter represents idle movements that are not goal-directed.

We observed that a subset of trials involved prolonged wiggling (duration > 1 second) and long reaction times (> 1.2 seconds), consistent with behavioral disengagement. These trials comprised 6.7% of the data and had a mean number of direction changes of $k = 8.68$.

To exclude disengaged behavior, we restricted subsequent analyses with k as the independent variable to trials with a duration up to 1 second (see Methods 4.2.1). Within this restricted dataset, we aim to distinguish between active sensing and change-of-mind hypotheses. Wiggle trials were relatively uncommon, and the proportion of trials decreases as k increases: (1) 60.1% in $k = 0$, (2) 18.1% in $k = 1$, (3) 12.4% in $k = 2$, (4) 4.8% in $k = 3$, and (5) 4.6% in $k \geq 4$. (**Figure 2f**). To achieve adequate statistical power, we pooled wheel movements with at least 4 directional changes into one group. We plotted k between 0 and 8 directional changes, which represents all the data.

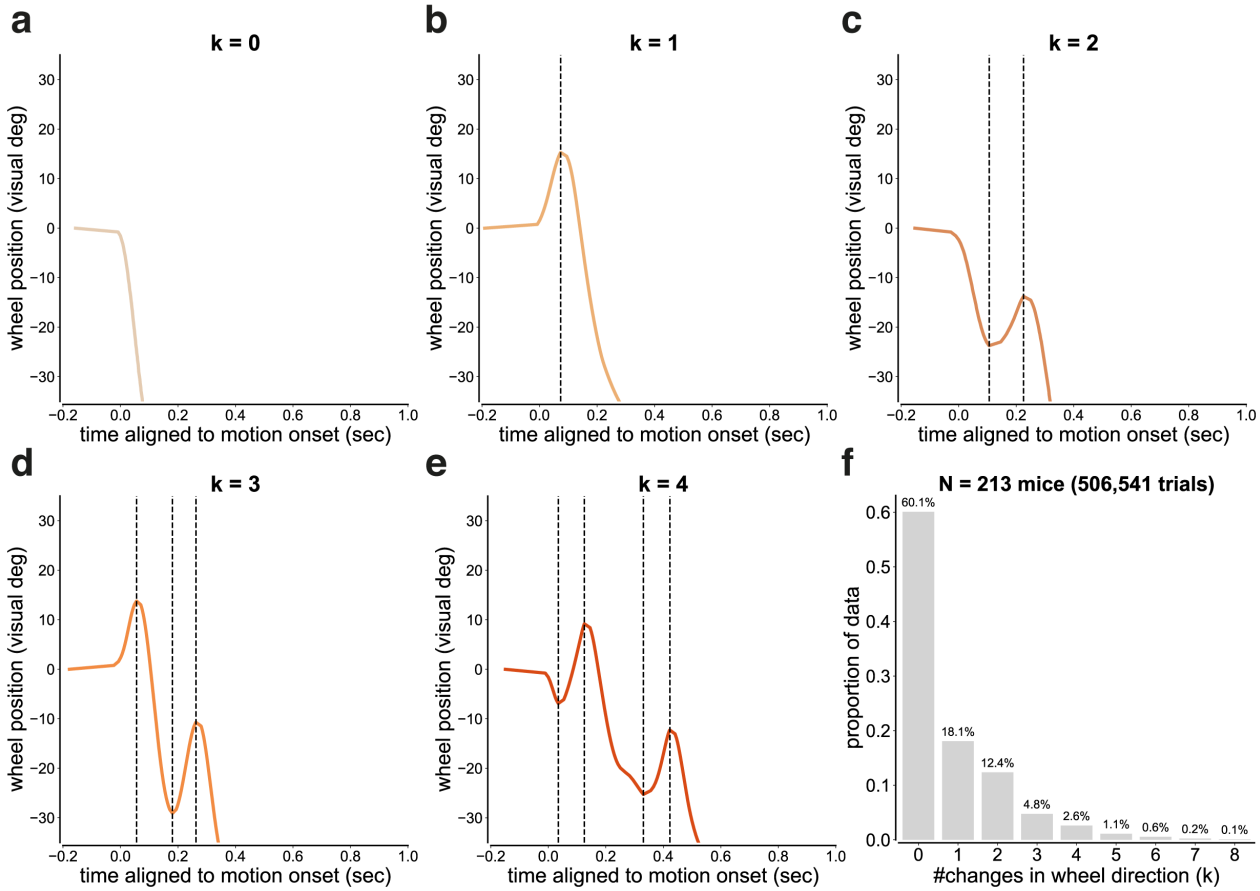

Figure 2: **Wiggles are wheel movements with multiple changes in wheel direction.** We computed the number of wheel directional changes (k) in each low visual stimulus contrast trial (6.25% contrast). Single-trial examples of wheel data (position versus time) for **(a)** $k = 0$, **(b)** $k = 1$, **(c)** $k = 2$, **(d)** $k = 3$, and **(e)** $k = 4$ directional changes. Each trial is aligned to motion onset, which is defined as the time when the wheel velocity exceeded the threshold of 0.5 radians/sec after a minimum of 0.05 seconds of quiescence. **(f)** Distribution of k from $506,541$ low visual stimulus contrast trials in 213 mice.

2.2 There is a positive relationship between mouse wiggles and low visual stimulus contrast accuracy.

To see if the low visual stimulus contrast accuracy changes with wiggles, we examined the relationship between motion energy and proportion correct as a function of visual stimulus contrast. If mice use wiggles to boost the salience of low-contrast stimuli, then wiggles increase the specrotemporal content available. Motion energy captures this spectrotemporal content, which the retina uses as an input. We expected that wiggles were most effective when the visual stimulus information was most limited.

We show that there is a strong, positive correlation between the motion energy and the low visual stimulus contrast accuracy (weighted linear regression, $R^2 = 0.949, p = 4.26 \times 10^{-5}, N = 8$ group medians from 213 mice) (**Figure 3a**). The best-fit line revealed a steep positive slope ($\beta = 0.0195$, 95% CI = [0.015, 0.024]), indicating that each unit increase in motion energy (10,000 $\text{deg}^2/\text{sec}^2$) was associated with a 1.95% improvement in low-contrast accuracy. Thus, mice that generated large, rapid changes in retinal image speed with the wheel were more successful during low-contrast trials.

This relationship was not seen in zero visual stimulus contrast trials, where the proportion correct was not significantly dependent on motion energy (weighted linear regression, $R^2 = 0.445, p = 0.071, N = 8$ group medians from 213 mice) (**Figure 3b**). Since zero visual stimulus contrast trials were rewarded based on the biased blocks (80/20 or 20/80), the proportion correct is greater than 50% ($0.8 \times 0.8 = 0.64$). This result serves as a negative control and shows that accuracy does not increase with motion energy in the absence of a visual stimulus.

To demonstrate that wiggles are an active sensing strategy, we computed the wiggle occurrence independent of proportion correct as a function of visual contrast. Wiggle occurrence is defined as the proportion of wheel movements with at least 2 directional changes ($k \geq 2$). We expected that wiggles were most frequent during zero-contrast and least frequent during high-contrast. We show that the wiggle occurrence decreases as visual stimulus contrast increases (weighted linear regression, $R^2 = 0.995, p = 1.66 \times 10^{-4}, N = 5$ group medians from 213 mice, **Figure 3c**), which is indicative of active sensing. The mean wiggle occurrence decreases from 0.73 ± 0.08 (0.0 contrast) to 0.53 ± 0.11 (1.0 contrast).

The wiggle occurrence is non-zero during high visual stimulus contrast trials (0.53 ± 0.11). This observation runs counter to the active sensing hypothesis, which posits that mice wiggle the wheel when visual information is limited. We hypothesized instead that mice may wiggle the wheel more when aroused, especially in high contrast conditions where decision certainty is minimal.

To address arousal as a confounding factor, we used indirect (wiggle amplitude and duration) and direct (pupil diameter) metrics. We expected that wiggle amplitude and duration would be greater during low-contrast trials and that pupil diameter would be largely independent of wiggles.

We computed the wiggle amplitude as a function of visual contrast. During low-contrast trials, we show that mice wiggle the wheel for 3.4 ± 0.8 visual degrees, which is about one-tenth of a complete trial (3.5/35 is 10%). The wiggle amplitude decreases as visual stimulus contrast increases (weighted linear regression, $R^2 = 0.995, p = 1.66 \times 10^{-4}, N = 5$ group medians from 213 mice, **Figure 3d**). Since wiggle amplitude is 70% greater during low-contrast trials (3.4 ± 0.8 visual degrees) compared to high-contrast trials (2.0 ± 0.7 visual degrees), this supports the hypothesis that wiggles are used to improve visual detection.

Next, we computed the wiggle duration as a function of visual contrast. Wiggle duration is defined as the total time spent in rapid, low-amplitude, back-and-forth wheel movements during a trial. This metric excludes periods of stillness or slow drift. We reasoned that if wiggles during low-contrast trials reflect active sensing, they should be sustained for longer durations, whereas brief wiggles during high-contrast trials would be more consistent with arousal-related jitter. We show that the wiggle duration decreases as visual stimulus contrast increases (weighted linear regression, $R^2 = 0.994, p = 1.91 \times 10^{-4}, N = 5$ group medians from 213 mice, **Figure 3e**). Wiggle duration decreases from 2.8 ± 1.4 seconds (0.0 contrast) to 0.95 ± 0.83 seconds (1.0 contrast), which is indicative of mice performing longer wheel jitters when stimulus information is limited.

We performed pupil analyses to directly control for arousal. First, we observed no significant differences in the mean pupil diameter between wiggles and non-wiggles in the 200 msec after stimulus onset (Mann-Whitney-Wilcoxon test, $p = 0.093, N = 1,472$ trials, 92 mice, **Figure 3f**). Second, the median cross-correlation between pupil diameter and wheel position was negligible ($Med = 0.01, \sigma = 0.12, N = 1,337$ wiggle trials, **Figure S1b**). Taken together, this suggests that wiggles cannot be explained by arousal.

Last, we performed a weighted linear regression between the number of changes in wheel direction (k) and proportion correct during low-contrast trials. Based on $R^2 \geq 0.1$, 104/213 mice show a positive slope (48.8%) and 52/213 show a negative slope (24.4%) (**Figure 3g**). The distribution of wiggle-related changes was not consistent with random variation: 104 mice that benefited had a median slope of +0.029 (IQR: [0.019, 0.043]), whereas 52 non-benefiting mice showed a median slope of -0.021 (IQR: [-0.017, -0.034]). Furthermore, 22% of all mice had an $R^2 \geq 0.7$, indicating that the effect was substantial for a sizeable fraction of the population. Benefiting mice were less impulsive and exhibited fewer false starts than non-benefiting mice (**Figure S6**). Together, these results indicate that the effect of wiggles is heterogeneous across the mouse population.

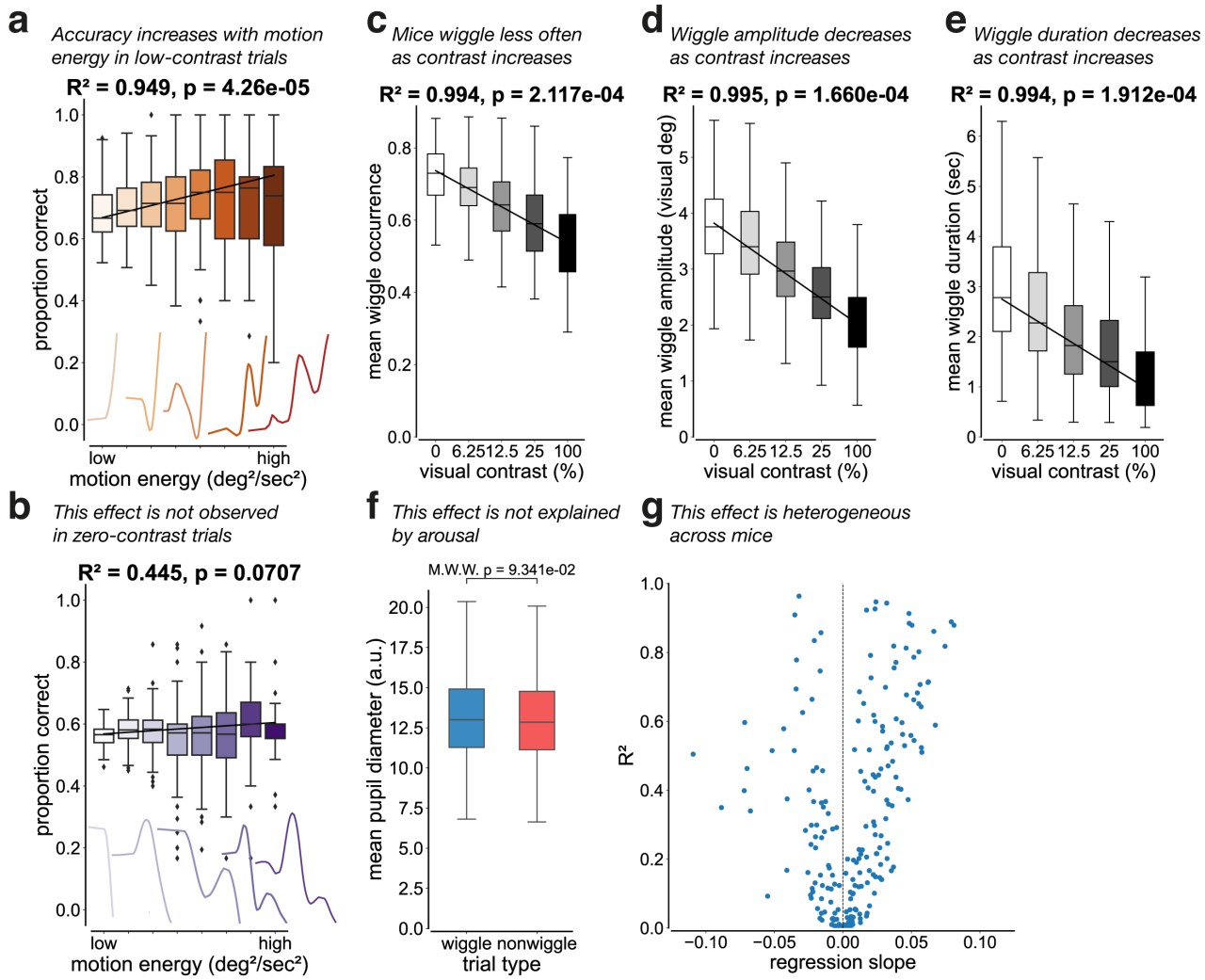

Figure 3: **There is a positive relationship between mouse wiggles and low visual stimulus contrast accuracy.** **(a - b)** Distributions of median proportion correct in binned motion energy data across 213 mice. Motion energy is defined as the time-averaged squared speed across segments, ranging from 500 to 80,500 $\text{deg}^2/\text{sec}^2$ (see Methods 4.2.4 and 4.2.7). Sessions with at least 3 trials for a given motion energy bin were included in this analysis. **(a)** As the motion energy increases, the low visual stimulus contrast accuracy increases (weighted linear regression, $R^2 = 0.949, F(1,6) = 111.4, p = 4.26 \times 10^{-5}, N = 8$ group medians from 213 mice). **(b)** The zero visual stimulus contrast accuracy is not significantly dependent on motion energy (weighted linear regression, $R^2 = 0.445, F(1,6) = 4.811, p = 0.129, N = 8$ group medians from 213 mice). **(c)** As the visual stimulus contrast increases, the mean wiggle occurrence significantly decreases (weighted linear regression, $R^2 = 0.994, F(1,3) = 474.6, p = 2.24 \times 10^{-5}, N = 5$ group medians from 213 mice). **(d)** As the visual stimulus contrast increases, the mean wiggle amplitude significantly decreases (weighted linear regression, $R^2 = 0.995, F(1,3) = 0.995, p = 1.66 \times 10^{-4}, N = 5$ group medians from 213 mice). **(e)** As the visual stimulus contrast increases, the mean wiggle duration significantly decreases (weighted linear regression, $R^2 = 0.994, F(1,3) = 508.1, p = 1.91 \times 10^{-4}, N = 5$ group medians from 213 mice). **(f)** The mean pupil diameter (a.u.) is comparable between wiggles and non-wiggles during the first 200 ms after stimulus onset (Mann-Whitney-Wilcoxon test, $U = 1.12 \times 10^6, p = 0.093, N = 1,472$ trials, 92 mice). **(g)** The relationship between weighted linear regression slope and R^2 is heterogeneous across 213 mice. The slope is computed from number of changes in wheel direction (k) versus proportion correct in low-contrast trials across sessions per mouse. Trials with a duration of up to 1 second were included in this analysis.

2.3 Mouse wiggles cannot be explained by change-of-mind.

To address change-of-mind as an alternative explanation for mouse wiggles during low visual stimulus contrast trials, perturbation experiments are necessary. We re-analyzed existing mouse behavioral data, which served as controls to disambiguate active sensing from change-of-mind.

First, we repeated the original analysis in **Figure 3c** for a dataset where the spatial frequency was halved by Ortiz et al, 2020. The Gabor patch spatial frequency was 0.05 cycles per degree, which is easier for mice to perceive than 0.10 cycles per degree and close to the preferred spatial frequency of the mouse visual system (Prusky et al, 2004). In a less visually demanding task, the mean number of movements per second was comparable between the highest contrast (64%) and lowest contrast (1.2%) conditions (Mann-Whitney-Wilcoxon two-sided test, $p = 0.040, N = 23$ closed-loop sessions, 7 mice, **Figure 4a**). Since contrast sensitivity depends jointly on visual contrast and spatial frequency, this finding suggests that when the spatial frequency is sufficiently low, mice no longer modulate their wiggling behavior as a function of contrast strength.

Second, we analyzed data from a task variant that differed in the following ways (Baruchin et al, 2023). (1) It was a visual discrimination task rather than a visual detection task. Mice were presented with two Gabor patches with unequal contrasts and received reward for using a wheel to center the higher contrast patch. (2) The visual stimulus onset and go-cue onset were not coincidental. Prior to the go-cue onset, the visual stimulus was uncoupled from the wheel (open-loop). Any wheel movements during this time were ignored. Thus, each trial consisted of an open-loop period ($0.2 - 0.5$ sec) and closed loop period ($0.4 - 0.8$ sec).

We expected that mice would wiggle less often during the open-loop period compared to the closed-loop period. When the wheel is disconnected from the visual stimulus, mice can no longer use wiggling to boost the salience of low-contrast stimuli. We hypothesized that mice would abandon an active sensing strategy when visuo-motor coupling was unavailable. Consistent with this prediction, we observed that mice wiggled significantly less often during the open-loop period in the lowest contrast condition (25%) (Wilcoxon paired samples test, $p = 5.59 \times 10^{-9}$, $N = 15$ sessions, 4 mice, **Figure 4b**). This result indicates that mouse wiggles are a function of visuo-motor coupling.

Third, we performed a similar comparison between open-loop and closed-loop task variants (Ortiz et al, 2020) with the following differences. (1) Only a relatively high-contrast visual stimulus (64%) was used. (2) During the open-loop task, the visual stimulus was dynamic and drifted at a temporal frequency of 1.5 Hz. We hypothesized that mice would wiggle less often during the open-loop task for the reason outlined above in addition to a second reason. Since the visual stimulus is moving, the mouse has does not need to wiggle the wheel to build optic flow during low-contrast trials.

Although the visual stimulus was not perceptually demanding in either loop condition, we observed that mice wiggled less often during the dynamic, open-loop task compared to the static, closed-loop task (Mann-Whitney-Wilcoxon two-sided test, $p = 2.21 \times 10^{-11}, N = 50$ open-loop sessions and 23 closed-loop sessions, 7 mice, **Figure 4c**). Taken together with **Figure 4b**, the open-loop perturbation experiments demonstrate that mouse wiggles cannot be explained by change-of-mind.

Last, we analyzed data from a task variant that manipulated visuo-motor gain (The International Brain Laboratory et al, 2021). During early shaping sessions, mice experienced double gain (1 wheel degree: 4 visual degrees) during 50% stimulus contrast trials. We compared correct trials between high gain (50% contrast) and low gain (6.25% contrast) conditions. We observed that the mean wiggle amplitude was greater during low visuo-motor gain sessions (1 wheel degree: 2 visual degrees) (Mann-Whitney-Wilcoxon two-sided test, $p = 5.80 \times 10^{-3}, N = 203$ mice, **Figure 4d**). The mean wiggle amplitude increased by 5.6% from 8.9 ± 1.6 visual degrees (higher gain) to 9.4 ± 1.5 visual degrees (lower gain).

This result is consistent with the active sensing hypothesis. If mice perform wiggles to improve visual detection, then the size of wiggles should scale with the visuo-motor gain (smaller wiggles at higher gain and larger wiggles at lower gain). Together with the open-loop findings (**Figure 4b–c**), this indicates that mouse wiggling reflects an active sensing strategy rather than a change-of-mind.

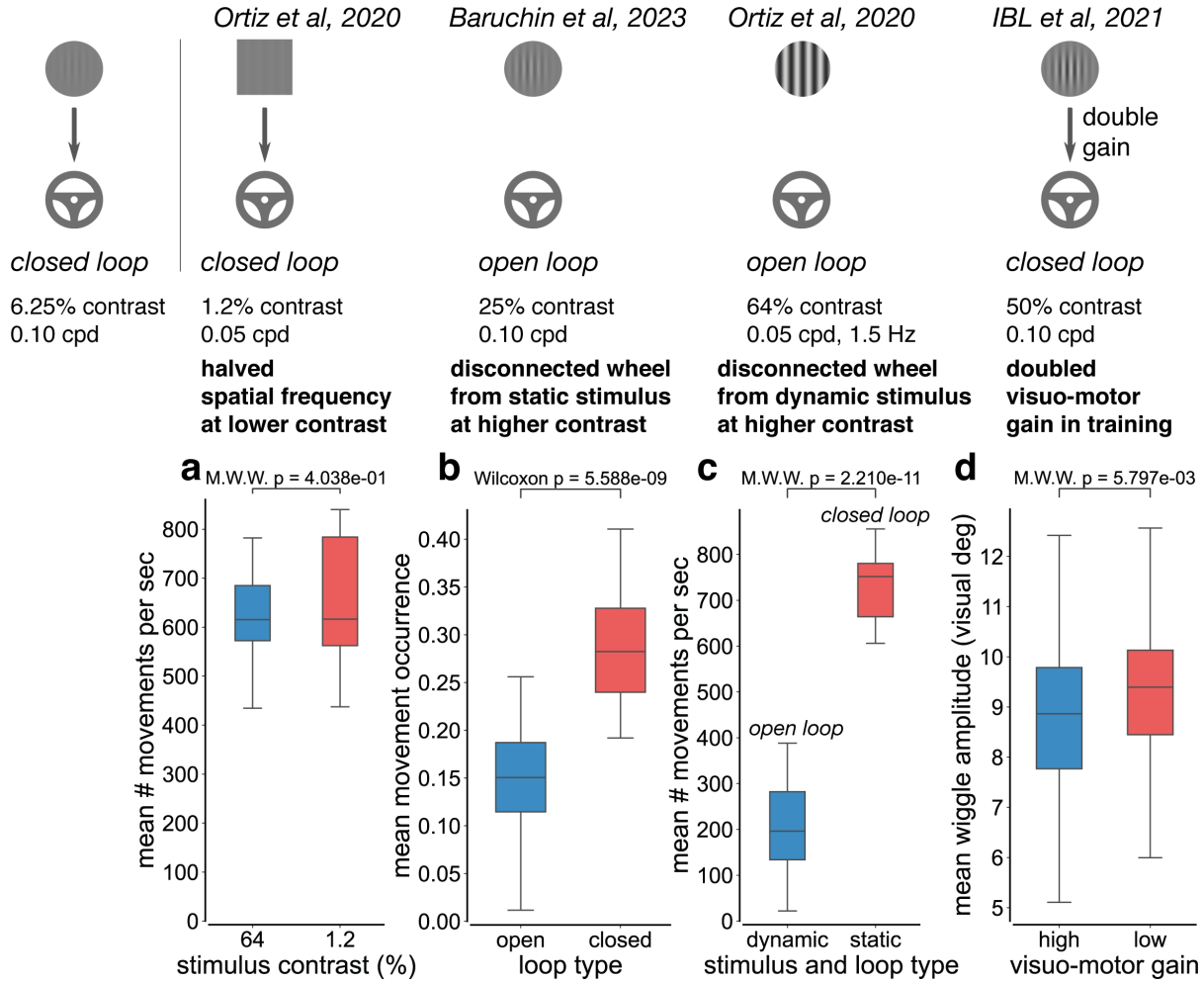

Figure 4: **Mouse wiggles cannot be explained by change-of-mind.** Variations of a visually-guided steering wheel task (Burgess et al, 2017) were used as controls. Movements were defined as times when the wheel velocity exceeded a threshold of 0.5 radians/sec after a minimum of 0.05 seconds of quiescence. **(a)** When the Gabor patch spatial frequency was 0.05 cyles per degree, the mean number of movements per second was not significantly dependent on stimulus contrast (data by Ortiz et al, 2020; Mann-Whitney-Wilcoxon two-sided test, $U = 226, p = 0.040, N = 23$ closed-loop sessions, 7 mice). **(b)** When mice performed a visual discrimination task, the mean movement occurrence significantly increased from open-loop to closed-loop periods (data by Baruchin et al, 2023; Wilcoxon paired samples test, $U = 2.0, p = 5.59 \times 10^{-9}$, $N = 15$ sessions, 4 mice). Each trial consisted of an open-loop period (the visual stimulus was uncoupled from the wheel prior to the go-cue onset) followed by a closed-loop period (the visual stimulus was coupled to the wheel after the go-cue onset). Mice were rewarded for using the wheel to center the higher contrast Gabor patch (25% versus 100% contrast trials). Any wheel movements between the stimulus onset and go-cue were ignored. **(c)** During 64% visual contrast trials with a spatial frequency of 0.05 cycles per degree, the mean number of movements per second increased from open-loop sessions with a dynamic stimulus (1.5 Hz) to closed-loop sessions with a static stimulus (data by Ortiz et al, 2020; Mann-Whitney-Wilcoxon two-sided test, $U = 14.0, p = 2.21 \times 10^{-11}, N = 50$ open-loop sessions and 23 closed-loop sessions, 7 mice). **(d)** When mice were learning the original task, the mean wiggle amplitude increased from correct 50% contrast trials early in training (high-gain sessions with 1 wheel degree: 4 visual degrees) to all 6.25% contrast trials late in training (low-gain sessions with 1 wheel degree: 2 visual degrees) (data by The International Brain Laboratory et al, 2021; Mann-Whitney-Wilcoxon two-sided test, $U = 174.0, p = 4.80 \times 10^{-2}, N = 25$ mice).

2.4 Mice wiggle the wheel at speeds that generate visual temporal frequencies close to the range of maximal contrast sensitivity.

To see if higher speed wiggles are more accurate, we examined whether low visual stimulus contrast accuracy depended on the temporal frequency generated by wiggles. Specifically, we quantified the relationship between visual temporal frequency and proportion correct as a function of the number of changes in wheel direction. Based on the mouse contrast sensitivity function, we expected wiggles to be most effective when they produced temporal frequencies near the range of maximal sensitivity.

First, we show that the number of changes in wheel direction (k) is negatively correlated with the temporal frequency of the visual stimulus (weighted linear regression, $R^2 = 0.758, p = 0.129, N = 8$ group medians from 213 mice, **Figure 5a**). Temporal frequency is highest during $k = 1$ movements (18.78 ± 3.05 Hz) and lowest during $k \geq 4$ movements (11.52 ± 2.45 Hz). We hypothesized that this negative correlation reflects a constraint imposed by mouse temporal contrast sensitivity: $k = 1$ movements may produce visual motion that is too fast to be perceptible by mice, whereas $k \geq 4$ movements may produce visual stimulus modulations that are within the range of mouse visual acuity.

To test this, we asked whether mice wiggle the wheel at a temporal frequency that aligns with the peak contrast sensitivity of the mouse visual system. We compared our behavioral data to a mouse temporal contrast sensitivity (TCS) curve (Umino et al, 2018). We found that the average temporal frequency during $k \geq 4$ wiggles (11.52 ± 2.45 Hz) closely matches the frequency at which mouse TCS peaks (12 Hz; TCS = 2.69, SEM = 0.36, **Figure 5b**). Although $k \geq 4$ wiggles represent a small proportion of the data (13.7%, **Figure 2f**), the overall dataset is large ($25,474$ trials from 213 mice), which provides sufficient power to estimate the average temporal frequency. Based on a one-sample t-test, the observed difference from the reference value (12 Hz) corresponds to a small effect size (Cohen's d = 0.196), with an estimated power of 81.2% at $\alpha = 0.05$. Taken together, these findings suggest that mice can perceive the left-to-right visual motion elicited by wiggle movements.

It is important to note that the TCS data is based on full-field visual stimulus whereas the wheel data is based on a local visual stimulus. In the study by Umino and colleagues, the TCS is equal to the sensitivity index of freely moving mice during a Go/No-Go task that manipulated temporal frequency at about the same spatial frequency (see Methods 4.2.9).

We also observed that the wiggle temporal frequency data is variable. For example, the standard deviation in $k \geq 4$ directional changes is large (2.45 Hz is about 20% of 11.52 Hz). This illustrates that wiggles are not periodic but vary in amplitude and duration within and across trials.

We asked what proportion of mice shows a positive relationship between visual temporal frequency and low visual stimulus contrast accuracy during $k \geq 4$ directional changes. Based on $R^2 \geq 0.1$, 50/199 mice show a positive slope (25.1%) and 39/199 mice show a negative slope (19.6%) (**Figure 5c**). This suggests that a subset of mice benefit from high visual temporal frequencies of about 12 Hz generated by wheel movement.

Next, we asked if higher visual temporal frequencies generated by mouse wiggles were more accurate for a given number of changes in wheel direction. We binned visual temporal frequency data for a fixed k and computed the low visual stimulus contrast accuracy across bins. For $k = 2$ trials, the correlation was weak and non-significant (weighted linear regression, $R^2 = 0.100, p = 0.446, N = 8$ group medians from 213 mice, **Figure 5d**), while stronger and statistically significant correlations emerged for $k = 3$ trials (weighted linear regression, $R^2 = 0.520, p = 0.043, N = 8$ group medians generated from 213 mice; **Figure 5e**) and $k \geq 4$ trials (weighted linear regression, $R^2 = 0.593, p = 0.025, N = 8$ group medians from 213 mice, **Figure 5f**).

The within-k analysis in **Figures 5d–f** is consistent with the across-k analysis in **Figure 5b** up to 12 Hz. **Figure 5b** shows that the median temporal frequencies in $k = 2$, $k = 3$, and $k \geq 4$ trials are close to the peak mouse TCS. In line with this, **Figures 5d–f** show that the proportion correct is above chance level up to 12 Hz.

However, an inconsistency emerges in the following temporal frequency bins: 15 Hz, 18 Hz, and 21 Hz. While **Figure 5b** predicts that proportion correct decreases at temporal frequencies above 12 Hz, **Figures 5d–f** do not show a drop in accuracy. We believe this inconsistency emerges because of a drop in data in those bins. For instance, there are $14,470$ trials at 12 Hz for $k \geq 4$, but only $8,735$ trials at 15 Hz, $5,205$ trials at 18 Hz, and $2,969$ trials at 21 Hz. This reduction in data likely limits the statistical power to detect a decline in accuracy at high temporal frequencies, even if such a decline is present.

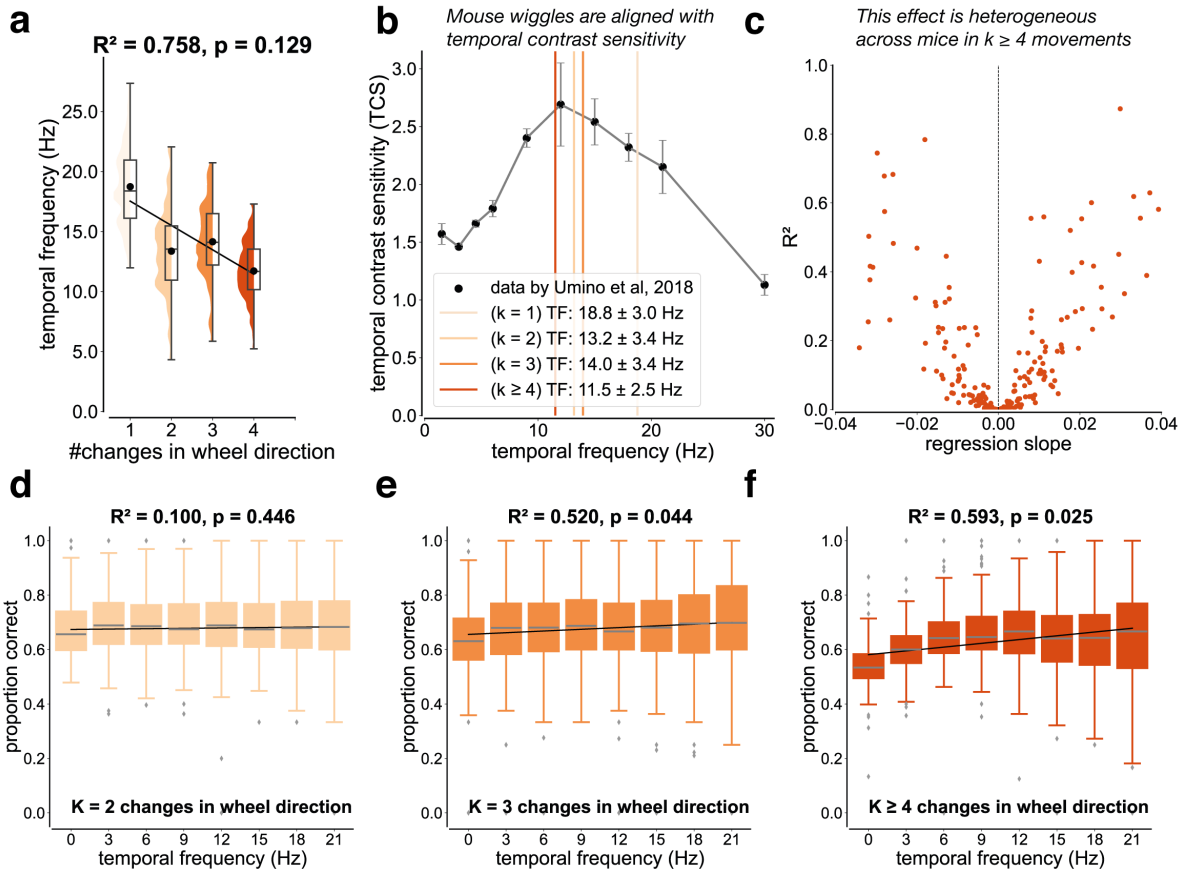

Figure 5: **Mice wiggle the wheel at speeds that generate visual temporal frequencies close to the range of maximal contrast sensitivity.** Visual temporal frequency is defined as the wheel speed divided by the stimulus spatial frequency (see Methods 4.2.5). Trials with $k = 0$ were excluded from this analysis. **(a)** Distribution of visual temporal frequency in binned wheel directional changes (k) data across 213 mice. As k increases, the visual temporal frequency decreases during low-contrast trials (weighted linear regression, $R^2 = 0.758, F(1.6) = 6.278, p = 0.129, N = 8$ group medians from 213 mice), although the trend is not significant. **(b)** During $k \geq 4$ directional changes, mice wiggle the wheel at 11.5 ± 2.5 Hz, which is near the temporal frequency with maximum temporal contrast sensitivity (indicated by a red line at 12 Hz from data by Umino et al, 2018). **(c)** The relationship between weighted linear regression slope and R^2 is heterogeneous across 199 mice. The slope is computed from visual temporal frequency versus k in low-contrast trials across sessions per mouse. Mice with at least 5 trials in each of the 8 visual temporal frequency bins were included in this analysis, which led to the exclusion of 14 mice. Performance analysis shows that: **(d)** During $k = 2$ directional changes, the proportion correct is independent of visual temporal frequency (weighted linear regression, $R^2 = 0.100, F(1, 6) = 0.665, p = 0.446, N = 8$ group medians from 213 mice). **(e)** During $k = 3$ directional changes, the proportion correct increases with visual temporal frequency (weighted linear regression, $R^2 = 0.520, F(1, 6) = 6.50, p = 0.043, N = 8$ group medians generated from 213 mice). **(f)** This relationship is strongest in $k \geq 4$ directional changes (weighted linear regression, $R^2 = 0.593, F(1, 6) = 8.753, p = 0.025, N = 8$ group medians from 213 mice).

2.5 Wiggle duration enhances visual stimulus side decoding accuracy in midbrain and thalamic regions.

To test if wiggles improve the detection of low visual contrast stimuli in neural data, we applied a logistic regression decoder analysis to single-trial, single-neuron electrophysiology data (The International Brain Laboratory, 2023). We hypothesized that stimulus side decoding would be more accurate during wiggle trials than non-wiggle trials. However, the input to a decoder needs to be the same length from both conditions, and a non-wiggle is much faster than a wiggle (movement duration of about 0.2 seconds versus 1 second). The ideal control is with long, non-wiggling durations that do not come from losing focus, motivation, or attention. The caveat is that such trials do not exist.

We instead asked if visual stimulus side decoding accuracy improves over the duration of a wiggle. We compared decoding accuracy between short (0.2 seconds) and long (1 second) wiggle durations across multiple brain areas.

We show that this is indeed the case in midbrain and thalamic regions. In the midbrain, both the superior colliculus (SC) and anterior pretectal nucleus (APN) showed significant improvements in decoding accuracy with longer wiggles (SC: $p < 0.001$, +3% accuracy; APN: $p < 0.001$, +5% accuracy, **Figure 6a**). Similarly, the lateral posterior nucleus of the thalamus (LP) exhibited a significant decoding enhancement ($p = 0.001$, +3% accuracy, **Figure 6b**). Positive control analyses in the primary motor cortex (MOp) confirmed expected improvements ($p = 0.001$, +2% accuracy, **Figure 6c**), whereas the negative control in auditory cortex (AUD) showed no significant change ($p = 0.124$, +1% accuracy, **Figure 6d**). These results demonstrate that extended wiggle duration selectively improves neural representations of stimulus side in subcortical regions, which is consistent with the hypothesis that longer wiggles provide more visual stimulus information than shorter wiggles.

It is important to note that decoding accuracy did not improve with longer wiggles in the primary visual cortex (V1: $p = 0.382$, -0.7% accuracy, **Figure S9**) but it did in the antero-medial primary visual area (VISa: $p = 0.035$, +2.2% accuracy, **Figure S9**). This aligns with an analysis of the proportion of neurons with increased firing during wiggles compared to non-wiggles 400 msec after stimulus onset (VISa: 16.67%, SC: 10.93%, V1: 8.37%) in 0.0625, 0.125, and 0.25 visual stimulus contrast trials (**Figure 7a**). This distribution changes in 0.0 visual stimulus contrast trials (VISa: 6.25%, SC: 18.01%, V1: 7.11%) in the absence of visual feedback (**Figure 7c**), which suggests that wiggle-related modulation in visual areas does not reflect an efference copy. Taken together, these results indicate that wiggling can be detected in the neural data.

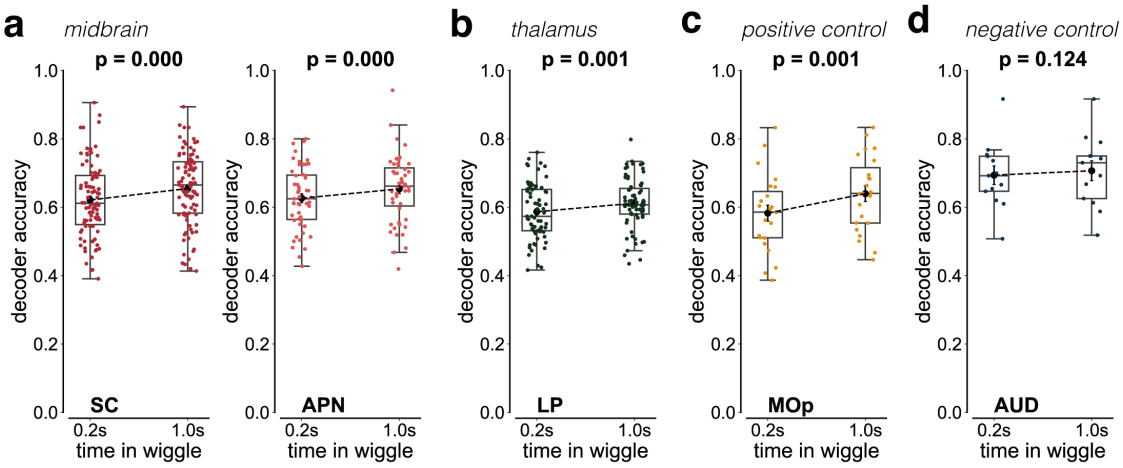

Figure 6: **Wiggle duration enhances stimulus side decoding accuracy in midbrain and thalamic regions.** We trained a logistic regression decoder to predict stimulus side (left or right) from neural activity in a given brain region as a function of wiggle duration (0.2 seconds versus 1 second). Single trial, single-neuron post-stimulus onset activity was used as an input (see Methods 4.1.2 and 4.2.8), including only trials with a visual stimulus contrast between 0% and 100%. Sessions with fewer than 20 wiggle trials were excluded. Neural data was binned in 20 msec windows, and decoding was repeated 100 times with stratified train-test splits. Brain region abbreviations and colors follow the Allen Institute Brain Atlas (SC: superior colliculus; APN: anterior pretectal nucleus; LP: lateral posterior nucleus of the thalamus; MOp: primary motor cortex; AUD: auditory cortex). All comparisons used a Wilcoxon signed-rank test ($\alpha = 0.05$). **(a)** Midbrain regions show significant improvements: SC ($p < 0.001, N = 91$ sessions, 3% improvement) and APN ($p < 0.001, N = 51$ sessions, 5% improvement). **(b)** Thalamic LP also shows significant improvement ($p = 0.001, N = 72$ sessions, 3% improvement). Controls confirm the specificity: **(c)** positive control MOp shows expected significant improvement ($p = 0.001, N = 23$ sessions, 2% improvement) while **(d)** negative control AUD shows no significant change ($p = 0.382, N = 25$ sessions, 1% improvement).

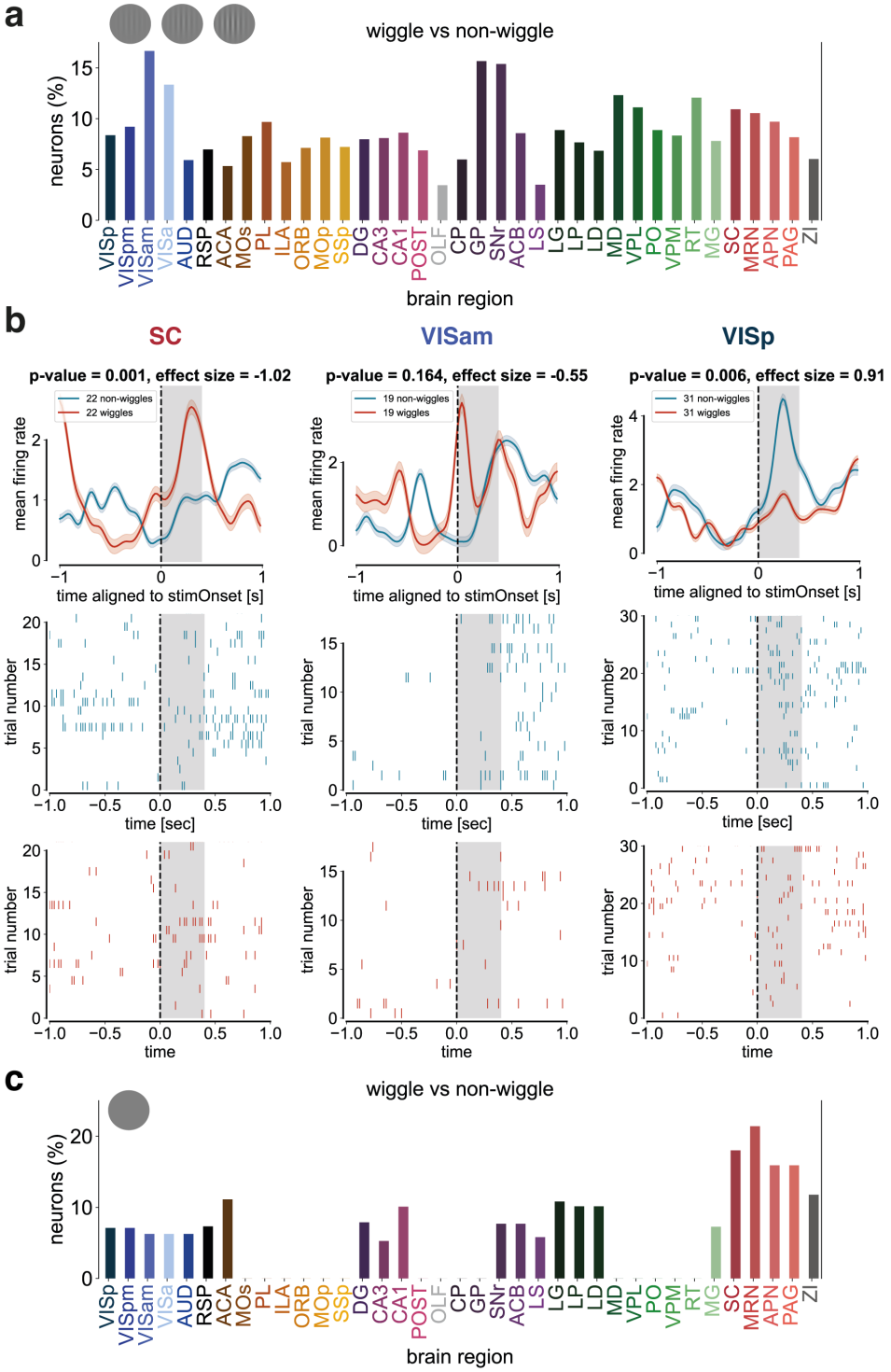

Figure 7: **Proportion of neurons with increased firing during wiggles versus non-wiggles 400 ms after visual stimulus onset. (a)** Across $N = 37$ brain regions, the fraction of neurons (%) with a significantly higher normalized mean firing rate during wiggles compared to non-wiggles is shown. Significance was defined as $p \leq 0.05$ (Wilcoxon signed-rank test) and Cohen's $d \geq 0.8$. Spikes were counted in 20 msec bins, smoothed with a Gaussian kernel ($\sigma = 3$ bins), and normalized by dividing by baseline firing rate (–0.5 to 0 s relative to stimulus onset) + 1 spike/s. To have enough wiggle trials for analysis, the 0.0625, 0.125, and 0.25 visual stimulus contrast trials were used. For each wiggle trial, the closest non-wiggle trial in session time was used for comparison. The highest proportion of neurons was observed in the antero-medial primary visual area (VISam: 16.67%), and the lowest in the olfactory area (OLF: 3.45%). Brain region abbreviations and colors follow the Allen Institute Brain Atlas. **(b)** Corresponding single-cell example responses aligned to visual stimulus onset for the superior colliculus (SC), antero-medial primary visual area (VISam), and primary visual cortex (VISp). **(c)** Corresponding negative control in zero visual stimulus contrast trials.

3 Discussion

Our first claim is that mouse wheel wiggling is an example of active sensing. This is supported by the significant positive relationship between low visual stimulus contrast accuracy and motion energy across 213 mice, which has a regression line that is statistically significantly different from zero ($R^2 = 0.949, p = 4.26 \times 10^{-5}$, **Figure 3a**). This effect is also seen with the number of changes in wheel direction ($R^2 = 0.810, p = 0.038$, **Figure S3a**) but the relationship is not as strong. Thus, the positive relationship between mouse wiggles and low-contrast accuracy is more obvious with a continuous metric (**Figure 3a**) than a discrete metric (**Figure S3a**) of wheel movement. Despite the heterogeneity of the mouse population (**Figure S4**) and relative uncommonness of wiggle trials (**Figure 2f**), we were still able to demonstrate a substantial positive correlation across mice.

The advantage of motion energy as a metric is that it is closest to what the retina takes as input. The retina responds to contrast within a spatiotemporal window. In addition, motion energy is not sensitive to trial duration while k is: there are disengaged wheel movements with hundreds of changes in wheel direction. Since motion energy is the time-averaged squared speed, it provides a measure of wiggle intensity that increases with both the magnitude and duration of rapid movements.

The advantage of k as a metric is that it is easy-to-use and intuitive. To remove disengaged trials, we restricted analyses with k as the independent variable to trials with a duration of up to 1 second. In this way, we were able to address evidence accumulation as an alternative explanation for mouse wheel wiggling by binning trials of similar durations and still observing the effect (**Figure S5b**).

Our second claim is that mouse wheel wiggling cannot be explained by arousal or change-of-mind. Since the mean pupil diameter is comparable between wiggles and non-wiggles (Mann-Whitney- Wilcoxon test, $U = 1.12 \times 10^6, p = 0.093, N = 1,472$ trials, 92 mice; **Figure 3f**) and the distribution of median cross-correlation coefficients between pupil data and wheel data ranges from -0.2 to 0.2 (**Figure S1b**), this effect cannot be explained by arousal. Moreover, there is a decrease in the proportion of wiggle trials when the wheel is uncoupled from the visual stimulus (data by Baruchin et al, 2023; Wilcoxon paired samples test, $p = 5.59 \times 10^{-9}, N = 15$ sessions, 4 mice, **Figure 4b**). This open-loop perturbation experiment demonstrates that wiggles cannot be explained by change-of-mind. Since the mean wiggle amplitude increases when the visuo-motor gain decreases (data by The International Brain Laboratory et al, 2021; Mann-Whitney-Wilcoxon two-sided test, $p = 4.80 \times 10^{-2}, N = 25$ mice, **Figure 4d**), this perturbation experiment provides further support for the argument that mouse wheel wiggling is an example of active sensing.

Our third claim is that mice wiggle the wheel at a natural temporal frequency for the visual system. Active sensing movements are often rapid compared to the speed of sensory transduction itself. Mouse wheel wiggling generates a median visual temporal frequency of 11.52 ± 2.45 Hz during $k \geq 4$ directional changes (**Figure 5a**), which is much higher than the $1-2$ Hz preferred temporal frequency of mouse V1 neurons (Marshel et al, 2011; Han et al, 2022). However, this visual temporal frequency aligns well with the maximum temporal contrast sensitivity identified by Umino and colleagues in a Go/No-Go task, which was 12 Hz (**Figure 5b**). This finding should be interpreted considering the limitations outlined in Methods 4.2.9, where the greatest caveat is the difference between full-field versus localized visual stimulus. We believe that these discrete, rapid, and repetitive wheel movements create large changes in sensory signals.

Our work highlights the role of active sensing in head-fixed mouse vision. While ethological studies of naturalistic mouse vision probe at the neural correlates of active eye and head movements (Parker et al, 2022; Sharp et al, 2025; Parker et al, 2025), it is much harder to do a cell-type specific interrogation of neural circuits in a freely-moving animal compared to a head-fixed animal. Recent advances in virtual reality technology combined with head-fixed recordings offer a promising alternative to measurements in freely moving animals (Judák et al, 2024; Isaacson et al, 2025). We demonstrate that head-fixed mice physically jitter a wheel during low visual contrast stimuli trials in the same spirit of humans performing fixational eye movements during high spatial frequency stimuli trials (Rucci et al, 2007), which are both active sensing strategies that serve to increase visual information.

Data analysis within and across mice revealed a substantial positive relationship between wiggles and low visual stimulus contrast accuracy. The large number of trials and animals in our dataset lends confidence to the robustness of the effect. We show that a subset of mice wiggles the wheel to boost the salience of low visual contrast stimuli. The salience of an object refers to its color, motion, shape, and brightness. Since the visual stimulus is always oriented vertically during the task, this means that when a mouse jitters the wheel left-to-right, it switches between black and white stripes as the low-contrast Gabor patch moves horizontally on the screen. By wiggling the wheel, head-fixed mice can build optic flow when stimulus information is limited during a visual perceptual decision-making task.

3.1 Limitations of the study

The task is designed to study priors, not active sensing.

Experimental factors likely contributed to the modest effect sizes observed in population-level analyses. First, most of the behavioral data was acquired during biased blocks. Since mice could exploit the block structure of the task rather than relying solely on the visual stimulus for decisions, this reduced their dependence on wiggles for perceptual enhancement (**Figure S5a**). Second, the spatial frequency of the visual stimulus was above the perceptible threshold. This meant that mice could perceive low visual contrast stimuli without wiggles. Redesigning the task to present more difficult visual stimuli at the perceptual threshold would likely reveal substantially larger benefits from wiggles. Third, the heterogeneous nature of wiggle responses across individual mice means that population averages obscure both the mice that benefit from wiggles and those that do not, diluting the overall effect size and masking the biological significance of this behavior. There are 110 mice with a monotonically increasing correlation, 24 mice with a monotonically decreasing correlation, and 69 mice with a non-monotonically increasing correlation (**Figure S4**).

The neural data is not retinotopically aligned to visual stimulus.

For cortical neurons in the retinotopic location of the visual stimulus, a moving visual stimulus would move from one neuron's receptive field to a second neuron's receptive field. This means that two neurons are excited at different times by the dynamic visual stimulus. Thus, a neural circuit mechanism of mouse wiggles likely involves sequentially activating neurons with retinotopically-aligned receptive fields to the visual stimulus. Since the neural data was acquired with a grid-like approach, it is non-trivial to understand the neural correlates of wiggles. We performed a preliminary analysis that shows decoding visual stimulus identity from neural activity improves with longer wiggles in midbrain and thalamic regions, including the superior colliculus (**Figures 6–7**). This is well-aligned with a recent study that demonstrates visual representations of active mouse eye saccades in the superior colliculus in head-fixed mice (Hunt et al, 2025).

A study by Millman and colleagues found that vasoactive intestinal peptide (VIP) interneurons in mouse V1 were sensitive to low-contrast nasal-to-temporal motion on the retina (Millman et al, 2020). Although this differs from how mouse wiggles move the visual stimulus (left-to-right versus front-to-back), it suggests that VIP interneurons contribute to processing low-contrast retinal motion.

4 Methods

4.1 Experimental model and subject details

All procedures and experiments were carried out in accordance with the local laws and following approval by the relevant institutions: the Animal Welfare Ethical Review Body at University College London; the Institutional Animal Care and Use Committees of Cold Spring Harbor Laboratory, Princeton University, University of Washington, University of California at Berkeley and University of California at Los Angeles; the University Animal Welfare Committee of New York University; and the Portuguese Veterinary General Board.

4.1.1 Mice

A total of 213 adult mice (C57BL6/J, 163 male, 50 female, age: 29.92 ± 13.47 weeks) were used for analysis. Mice were kept in a 12-hour light-dark cycle and performed the task in the dark period (from 7:00 to 19:00). Details are available here: (Appendix 1 of The International Brain Laboratory, 2021).

4.1.2 Electrophysiological data

Spike counts were obtained by summing spikes across time for both wiggle and non-wiggle trials. The neural data matrix had dimensions $N \times T \times K$, corresponding to N neurons, T time bins, and K trials, with indices $n = 1, \ldots, N$ and $t = 1, \ldots, T$. The bin size was 0.02 seconds. The input to the logistic regression decoder was the single-trial neural activity, given by:

$$X \in \mathbb{R}^{K \times (N \times T)} \tag{1}$$

Each input vector to the logistic regression decoder is a flattened neural population activity per trial reshaped to a row vector of length $N \cdot T$:

$$x^{(i)} \in \mathbb{R}^{(N \times T)}, i = 1, \ldots, K$$

	time window aligned to stimulus onset (sec)
post-stimulus decoder	$[0, 0.2]$ and $[0, 1]$

Table 2: We performed decoder analysis in the time windows above.

4.2 Quantitative and statistical analysis

4.2.1 Inclusion criteria for analysis

Trial Trials with a go-cue onset and visual stimulus onset within 0.05 seconds and a reaction time between 0.08 and 1.2 seconds were included in this analysis. In analyses with k as the independent variable, an additional criterion restricted the duration to 1 second.

Session Sessions with a minimum of 1 trial in each group were included in this analysis unless otherwise stated. There were 5 groups based on number of changes in wheel direction: (1) $k = 0$, (2) $k = 1$, (3) $k = 2$, (4) $k = 3$, and (5) $k \geq 4$.

Insertion Electrode insertions with a maximum of 80 microns of drift and a minimum of 10 units were included in this analysis.

4.2.2 Psychometric curves

To obtain a psychometric curve, data points were fitted with the following parametric error function, using a maximum likelihood procedure:

$$P = \gamma + (1 - \gamma - \lambda) \frac{erf\left(\frac{c-\mu}{\sigma}\right)}{2} \tag{2}$$

P probability of rightward choice

c visual stimulus contrast (%)

γ lapse rate for left visual stimuli

λ lapse rate for right visual stimuli

μ	response bias
σ	contrast threshold

A detailed psychometric curve fitting procedure is in Protocol 2 (The International Brain Laboratory, 2020b).

The **lapse rate** (λ) is defined as the probability of an incorrect response independent of the visual stimulus contrast (Prins et al, 2012). It captures the difference between observed performance and perfect performance at the asymptotes (Gupta et al, 2024).

4.2.3 Definition of wiggles

Wiggles are defined as movements with greater than or equal to 2 changes in wheel direction from trial start (pre-quiescent duration) to end (feedback time). A change in wheel direction is defined as an extremum in the wheel position (deg) vs time (sec) data.

Note: An equivalent analysis was done such that a change in wheel direction is defined as a sign change in the wheel velocity (deg/sec) vs time (sec) data.

4.2.4 Definition of motion energy

Motion energy is defined as the time-averaged squared speed across each pair of extrema in wheel position (deg) vs time (sec):

$$\begin{cases} \frac{1}{t_k - t_0} \sum_{i=0}^{k-1} \frac{|\theta_{i+1} - \theta_i|^2}{t_{i+1} - t_i} & k \neq 0 \\ \left(\frac{\theta_f - \theta_0}{t_f - t_0}\right)^2 & k = 0 \end{cases} \tag{3}$$

k	total number of extrema
θ_0	position of motion onset (deg)
θ_f	position of feedback (deg)
t_0	time of motion onset (sec)
t_f	time of feedback (sec)

Motion energy is in units of $\text{deg}^2/\text{sec}^2$ and ranges from 500 to 80,500 $\text{deg}^2/\text{sec}^2$. For each trial, we summed the squared positional changes between consecutive extrema divided by their corresponding time intervals (deg^2/sec). This value was then normalized by the total wiggle duration (sec) to obtain a time-averaged measure of movement intensity. To exclude ballistic movements that often follow wiggles in $k \neq 0$ trials, we performed analysis up to $k-1$ intervals rather than k intervals.

4.2.5 Definition of wiggle speed

Wiggle speed is defined as the total angular distance between each pair of extrema divided by the total wiggle duration in wheel position (deg) vs time (sec):

$$v = \begin{cases} \frac{1}{t_k - t_0} \sum_{i=0}^{k-1} |\theta_{i+1} - \theta_i| & k \neq 0 \\ \frac{|\theta_f - \theta_0|}{t_f - t_0} & k = 0 \end{cases} \tag{4}$$

To connect the wheel movement to visual stimulus movement, we first converted wheel speed (in wheel degrees per second) to visual stimulus speed (in visual degrees per second). The conversion factor was 1 wheel degree is about 2 visual degrees (0.3 wheel radians equal 35 visual degrees). Next, we divided the visual speed by the spatial frequency of the Gabor patch (0.1 cycles per degree) to obtain the effective temporal frequency experienced by the mouse. This temporal frequency reflects how rapidly the stimulus pattern drifted across the retina as the mouse wiggled the wheel. Thus, the visual temporal frequency is defined as the wiggle speed divided by the stimulus spatial frequency.

4.2.6 Definition of visual angle

Visual angle is the perceived size of a stimulus given by:

$$\phi = 2\arctan\left(\frac{h}{2d}\right) \tag{5}$$

h height of monitor (cm)

d distance between mouse and monitor (cm)

ϕ visual angle (deg)

Mice viewed a Gabor patch on a screen size of 246 mm diagonal active display area and were positioned 8 cm away from the screen to achieve 102 visual degrees azimuth (The International Brain Laboratory, 2021). The Gabor patch size is 19.7 cm if $\phi = 102^{\circ}$ and $d = 8$ cm.

Visual angle represents the size of an object's image on the retina. To obtain visual angle, we converted from wheel degrees to visual degrees. 35 visual degrees equals 17.2 wheel degrees (0.3 radians). Thus, 2 visual degrees correspond to about 1 wheel degree.

4.2.7 Weighted linear regression analysis

First, we binned the motion energy data across sessions per mouse to obtain a distribution of the proportion correct for a given visual contrast level. Each data point represented one session. We performed a linear regression between median proportion correct and motion energy across 8 bins per mouse, which was weighted by the number of trials across sessions. Second, we pooled the median proportion correct per motion energy bin across 213 mice. Each data point represented one mouse. We performed a linear regression between median proportion correct and motion energy across 8 bins in 213 mice, which was weighted by the number of sessions across mice.

Note: We performed weighted linear regression on 8 aggregated medians from 213 mice to avoid p-value inflation. When we used individual mice (hundreds) or sessions/trials (thousands) as regression points, we obtained spuriously small p-values because of large sample sizes. Therefore, all population-level regression analyses were based on aggregated medians across mice.

4.2.8 Decoder analysis

The logistic regression decoder maps the input neural activity to the probability of a binary outcome (i.e. left or right stimulus):

$$P\left(stimulus = right \mid x\right) = \frac{1}{1 + e^{-\beta_0 + \sum_{i=1}^{n} \beta_i x_i}} \tag{6}$$

$x = [x_1, x_2, \ldots, x_n]$ is the input vector containing neural activity. For $[0, 0.2]$ seconds of data with a bin size of 0.02 seconds, there are $n = 10$ time bins. Each x_i represents the neural activity in one time bin.

β_0 intercept term of the logistic regression

β_i weight associated with the ith time bin, indicating how strongly the activity in that time bin contributes to predicting choice

$P\left(stimulus = right \mid x\right)$ probability of the right choice given the neural activity

The decoder output is binary:

- Right if $P\left(stimulus = right \mid x\right) > 0.5$
- Left otherwise

The weights $(\beta_0, \beta_1, \ldots, \beta_n)$ are learned during model training by fitting the logistic regression model to maximize the likelihood of observed data (choices). For K trials, the likelihood function is:

$$\mathcal{L}\left(\beta\right) = \prod_{i=1}^{K} P\left(y_i \mid x_i, \beta\right)$$

$y_i \in \{0, 1\}$ stimulus side for trial i (i.e. left = 0 and right = 1)

x_i neural activity for trial i

$P(y_i = 1 \mid x_i, \beta) = \frac{1}{1+e^{-(\beta_0 + x_i \cdot \beta)}}$ logistic regression equation for probability of the correct stimulus side given the neural activity

Since it is easier to manipulate data as sums rather than products (i.e. for derivatives), we use the log-likelihood function:

$$\ell(\beta) = \sum_{i=1}^{N} \left[y_i \log P(y_i \mid x_i, \beta) + (1 - y_i) \log (1 - P(y_i \mid x_i, \beta)) \right] \tag{7}$$

We can substitute the logistic function in Equation 8:

$$P(y_i \mid x_i, \beta) = \frac{1}{1 + e^{-(\beta_0 + x_i \cdot \beta)}}$$

$$\ell(\beta) = \sum_{i=1}^{N} \left[y_i \log \left(\frac{1}{1 + e^{-(\beta_0 + x_i \cdot \beta)}} \right) + (1 - y_i) \log \left(1 - \frac{1}{1 + e^{-(\beta_0 + x_i \cdot \beta)}} \right) \right]$$

$$\ell(\beta) = \sum_{i=1}^{N} \left[y_i (\beta_0 + x_i \cdot \beta) - \log \left(1 + e^{-(\beta_0 + x_i \cdot \beta)} \right) \right]$$

The optimal parameters for $\beta = [\beta_1, \beta_2, \ldots, \beta_n]$ are found by maximizing the log-likelihood function. The goal is to obtain weights for a logistic regression model that produces probabilities aligned with the observed data.

4.2.9 Computation of Temporal Contrast Sensitivity

A behavioral d' was used to measure temporal contrast sensitivity (TCS):

$$d' = z(Hit) - z(FA) \tag{8}$$

$z(Hit)$ z-score of the probability of hits

$z(FA)$ z-score of the probability of false alarms

Temporal contrast sensitivity is a function of temporal frequency, spatial frequency, and background mean illumination (screen brightness). Screen brightness was not well-standardized across laboratories and no published value for illumination is listed (The International Brain Laboratory, 2021). On average, we determined that the screen brightness was 29.4 cd m^{-2}. This means that $\log(29.4) = 1.47$ log cd m^{-2}. Therefore, we used the data under photopic (1.80 log cd m^{-2}) conditions (See **Figure 2b** of Umino et al, 2008; **Figure 6f** of Umino et al, 2018) for details of mouse temporal contrast sensitivity analysis).

visual stimulus properties	The International Brain Laboratory, 2021	Umino et al, 2018
size	local	full field
contrast	6.25%	50%
spatial frequency	0.1 cycles per degree	0.128 cycles per degree
brightness	1.47 log cd m^{-2}	1.80 log cd m^{-2}

Table 3: These are caveats in the interpretation of mouse temporal contrast sensitivity.

Data Availability

Please follow these instructions to download the data. There are visualizations available to understand the data (Birman et al, 2024).

Code Availability

Please visit our Github repository to access the code used to produce the main results and figures presented in this manuscript. This International Brain Lab Github repository also contains code for brain-wide neural data analysis.

Acknowledgements

This work was supported by the Gatsby Charitable Foundation (GAT3755). Computational resources were provided by University College London. We thank the Kavli Institute of Theoretical Physics for providing the environment to prepare this manuscript (NSF PHY-2309135). We thank Alec Ortiz and Sylvia Schröder for perturbation experiment data. We thank Thomas Mrsic-Flogel, Peter Latham, Samuel Solomon, Adil Khan, Dimitar Kostadinov, and David Kleinfeld for comments on the behavioral and neural data analysis. We thank Joel E. Cohen for comments on the statistical analysis. We thank Peter Dayan, Anne Churchland, Andrew Peters, Viktor Roytman, and Alvin Zhang for comments on the manuscript. Most of all, we are indebted to Laurence F. Abbott for seeing this manuscript to completion.

Author Contributions

N.G. conceived the project, performed the data analysis, and wrote the manuscript.

Declaration of generative AI and AI-assisted technologies in the writing process

During the preparation of this work, we used Claude and ChatGPT to revise text and debug code. After using this tool/service, we reviewed and edited the content as needed and we take full responsibility for the content of the publication.

5 References

1. The International Brain Laboratory et al. Standardized and reproducible measurement of decision-making in mice. eLife 10, e63711 (2021).

2. Umino, Y., Pasquale, R. & Solessio, E. Visual Temporal Contrast Sensitivity in the Behaving Mouse Shares Fundamental Properties with Human Psychophysics. eNeuro 5, (2018).

3. Kato, S. et al. Global Brain Dynamics Embed the Motor Command Sequence of Caenorhabditis elegans. Cell 163, 656–669 (2015).

4. Fenk, L. M. et al. Muscles that move the retina augment compound eye vision in Drosophila. Nature 612, 116–122 (2022).

5. Wang, Z. J., Melfi, J. & Leonardo, A. Recovery mechanisms in the dragonfly righting reflex. Science 376, 754–758 (2022).

6. Kurnikova, A., Moore, J. D., Liao, S.-M., Deschênes, M. & Kleinfeld, D. Coordination of Orofacial Motor Actions into Exploratory Behavior by Rat. Curr. Biol. 27, 688–696 (2017).

7. Liao, S.-M. & Kleinfeld, D. A change in behavioral state switches the pattern of motor output that underlies rhythmic head and orofacial movements. Curr. Biol. 33, 1951-1966.e6 (2023).

8. Zhaoping, L. A new framework for understanding vision from the perspective of the primary visual cortex. Curr. Opin. Neurobiol. 58, 1–10 (2019).

9. Rucci, M., Iovin, R., Poletti, M. & Santini, F. Miniature eye movements enhance fine spatial detail. Nature 447, 852–855 (2007).

10. Intoy, J. & Rucci, M. Finely tuned eye movements enhance visual acuity. Nat. Commun. 11, 795 (2020).

11. Zhao, Z., Ahissar, E., Victor, J. D. & Rucci, M. Inferring visual space from ultra-fine extra-retinal knowledge of gaze position. Nat. Commun. 14, 269 (2023).

12. Mitchell, J. F., Reynolds, J. H. & Miller, C. T. Active Vision in Marmosets: A Model System for Visual Neuroscience. J. Neurosci. 34, 1183–1194 (2014).

13. Xiao, W., Sharma, S., Kreiman, G. & Livingstone, M. S. Feature-selective responses in macaque visual cortex follow eye movements during natural vision. Nat. Neurosci. 27, 1157–1166 (2024).

14. Singh, V. P., Li, J., Dawson, K., Mitchell, J. F. & Miller, C. T. Active vision in freely moving marmosets using head-mounted eye tracking. Proc. Natl. Acad. Sci. 122, e2412954122 (2025).

15. Diamond, M. E., von Heimendahl, M., Knutsen, P. M., Kleinfeld, D. & Ahissar, E. 'Where' and 'what' in the whisker sensorimotor system. Nat. Rev. Neurosci. 9, 601–612 (2008).

16. Kleinfeld, D. & Deschênes, M. Neuronal Basis for Object Location in the Vibrissa Scanning Sensorimotor System. Neuron 72, 455–468 (2011).

17. Shusterman, R., Smear, M. C., Koulakov, A. A. & Rinberg, D. Precise olfactory responses tile the sniff cycle. Nat. Neurosci. 14, 1039–1044 (2011).

18. Wachowiak, M. All in a Sniff: Olfaction as a Model for Active Sensing. Neuron 71, 962–973 (2011).

19. Moore, J. D. et al. Hierarchy of orofacial rhythms revealed through whisking and breathing. Nature 497, 205–210 (2013).

20. Takatoh, J. et al. The whisking oscillator circuit. Nature 609, 560–568 (2022).

21. Kaku, H. et al. A brainstem map of orofacial rhythms. 2025.01.27.635041 Preprint at https://doi.org/10.1101/2025.01.27.63 (2025).

22. Skyberg, R. J. & Niell, C. M. Natural visual behavior and active sensing in the mouse. Curr. Opin. Neurobiol. 86, 102882 (2024).

23. Yilmaz, M. & Meister, M. Rapid Innate Defensive Responses of Mice to Looming Visual Stimuli. Curr. Biol. 23, 2011–2015 (2013).

24. De Franceschi, G., Vivattanasarn, T., Saleem, A. B. & Solomon, S. G. Vision Guides Selection of Freeze or Flight Defense Strategies in Mice. Curr. Biol. 26, 2150–2154 (2016).

25. Hoy, J. L., Bishop, H. I. & Niell, C. M. Defined Cell Types in Superior Colliculus Make Distinct Contributions to Prey Capture Behavior in the Mouse. Curr. Biol. 29, 4130-4138.e5 (2019).

26. Boone, H. C. et al. Natural binocular depth discrimination behavior in mice explained by visual cortical activity. Curr. Biol. 31, 2191-2198.e3 (2021).

27. He, Y., Nieto, A. C., Blot, A. & Znamenskiy, P. A depth map of visual space in the primary visual cortex. 2024.09.27.615442 Preprint at https://doi.org/10.1101/2024.09.27.615442 (2024).

28. Parker, P. R. L. et al. A dynamic sequence of visual processing initiated by gaze shifts. Nat. Neurosci. 26, 2192–2202 (2023).

29. Sharp, S. L., Shin, J., Martins, D. M., Jones, K. & Niell, C. M. Neural dynamics in superior colliculus of freely moving mice. Cell Rep. 44, (2025).

30. Skyberg, R., Tanabe, S., Chen, H. & Cang, J. Coarse-to-fine processing drives the efficient coding of natural scenes in mouse visual cortex. Cell Rep. 38, (2022).

31. Niell, C. M. & Stryker, M. P. Modulation of Visual Responses by Behavioral State in Mouse Visual Cortex. Neuron 65, 472–479 (2010).

32. Keller, G. B., Bonhoeffer, T. & Hübener, M. Sensorimotor Mismatch Signals in Primary Visual Cortex of the Behaving Mouse. Neuron 74, 809–815 (2012).

33. Ayaz, A., Saleem, A. B., Schölvinck, M. L. & Carandini, M. Locomotion Controls Spatial Integration in Mouse Visual Cortex. Curr. Biol. 23, 890–894 (2013).

34. Saleem, A. B., Ayaz, A., Jeffery, K. J., Harris, K. D. & Carandini, M. Integration of visual motion and locomotion in mouse visual cortex. Nat. Neurosci. 16, 1864–1869 (2013).

35. Stringer, C. et al. Spontaneous behaviors drive multidimensional, brainwide activity. Science 364, eaav7893 (2019).

36. Dadarlat, M. C. & Stryker, M. P. Locomotion Enhances Neural Encoding of Visual Stimuli in Mouse V1. J. Neurosci. 37, 3764–3775 (2017).

37. Dipoppa, M. et al. Vision and Locomotion Shape the Interactions between Neuron Types in Mouse Visual Cortex. Neuron 98, 602-615.e8 (2018).

38. Meyer, A. F., O'Keefe, J. & Poort, J. Two Distinct Types of Eye-Head Coupling in Freely Moving Mice. Curr. Biol. CB 30, 2116-2130.e6 (2020).

39. Bouvier, G., Senzai, Y. & Scanziani, M. Head Movements Control the Activity of Primary Visual Cortex in a Luminance-Dependent Manner. Neuron 108, 500-511.e5 (2020).

40. Guitchounts, G., Masís, J., Wolff, S. B. E. & Cox, D. Encoding of 3D Head Orienting Movements in the Primary Visual Cortex. Neuron 108, 512-525.e4 (2020).

41. Parker, P. R. L., Abe, E. T. T., Leonard, E. S. P., Martins, D. M. & Niell, C. M. Joint coding of visual input and eye/head position in V1 of freely moving mice. Neuron 110, 3897-3906.e5 (2022).

42. King, C. W., Ledochowitsch, P., Buice, M. A. & Vries, S. E. J. de. Saccade-Responsive Visual Cortical Neurons Do Not Exhibit Distinct Visual Response Properties. eNeuro 10, (2023).

43. Dombeck, D. A., Khabbaz, A. N., Collman, F., Adelman, T. L. & Tank, D. W. Imaging Large-Scale Neural Activity with Cellular Resolution in Awake, Mobile Mice. Neuron 56, 43–57 (2007).

44. Bennett, C., Arroyo, S. & Hestrin, S. Subthreshold Mechanisms Underlying State-Dependent Modulation of Visual Responses. Neuron 80, 350–357 (2013).

45. Neske, G. T., Nestvogel, D., Steffan, P. J. & McCormick, D. A. Distinct waking states for strong evoked responses in primary visual cortex and optimal visual detection performance. J. Neurosci. https://doi.org/10.1523/JNEUROS 18.2019 (2019) doi:10.1523/JNEUROSCI.1226-18.2019.

46. Hulsey, D., Zumwalt, K., Mazzucato, L., McCormick, D. A. & Jaramillo, S. Decision-making dynamics are predicted by arousal and uninstructed movements. Cell Rep. 43, (2024).

47. Yin, C. et al. Spontaneous movements and their relationship to neural activity fluctuate with latent engagement states. Neuron 113, 3048-3063.e5 (2025).

48. Sun, H., Rüttiger, L. & Lee, B. B. The spatiotemporal precision of ganglion cell signals: a comparison of physiological and psychophysical performance with moving gratings. Vision Res. 44, 19–33 (2004).

49. Schottdorf, M. & Lee, B. B. A quantitative description of macaque ganglion cell responses to natural scenes: the interplay of time and space. J. Physiol. 599, 3169–3193 (2021).

50. Moore, T., Armstrong, K. M. & Fallah, M. Visuomotor Origins of Covert Spatial Attention. Neuron 40, 671–683 (2003).

51. Goldberg, M. E. & Wurtz, R. H. Activity of superior colliculus in behaving monkey. II. Effect of attention on neuronal responses. J. Neurophysiol. 35, 560–574 (1972).

52. Hafed, Z. M., Chen, C.-Y., Tian, X., Baumann, M. P. & Zhang, T. Active vision at the foveal scale in the primate superior colliculus. J. Neurophysiol. 125, 1121–1138 (2021).

53. Ambrad Giovannetti, E. & Rancz, E. Behind mouse eyes: The function and control of eye movements in mice. Neurosci. Biobehav. Rev. 161, 105671 (2024).

54. Kang, I., Talluri, B. C., Yates, J. L., Niell, C. M. & Nienborg, H. Is the impact of spontaneous movements on early visual cortex species specific? Trends Neurosci. 48, 7–21 (2025).

55. Gulbinaite, R. et al. Spatiotemporal resonance in mouse primary visual cortex. Curr. Biol. 34, 4184-4196.e7 (2024).

56. Fulvio, J. M., Miao, H. & Rokers, B. Head jitter enhances three-dimensional motion perception. J. Vis. 21, 12 (2021).

57. Palmisano, S., Pinniger, G. J., Ash, A. & Steele, J. R. Effects of Simulated Viewpoint Jitter on Visually Induced Postural Sway. Perception 38, 442–453 (2009).

58. Watson, L. M. et al. Image Jitter Enhances Visual Performance when Spatial Resolution Is Impaired. Invest. Ophthalmol. Vis. Sci. 53, 6004–6010 (2012).

59. Musall, S., Kaufman, M. T., Juavinett, A. L., Gluf, S. & Churchland, A. K. Single-trial neural dynamics are dominated by richly varied movements. Nat. Neurosci. 22, 1677–1686 (2019).

60. Kaufman, M. T., Churchland, M. M., Ryu, S. I. & Shenoy, K. V. Vacillation, indecision and hesitation in moment-by-moment decoding of monkey motor cortex. eLife 4, e04677 (2015).

61. Rolfs, M., Schweitzer, R., Castet, E., Watson, T. L. & Ohl, S. Lawful kinematics link eye movements to the limits of high-speed perception. Nat. Commun. 16, 3962 (2025).

62. Huang, X., Ghimire, B., Chakrala, A. S. & Wiesner, S. Neural coding of multiple motion speeds in visual cortical area MT. eLife 13, (2025).

63. Laboratory, I. B. Behavior: Appendix 2: IBL protocol for mice training. Preprint at https://doi.org/10.6084/m9.figshare.11 (2022).

64. Ortiz, A. V., Aziz, D. & Hestrin, S. Motivation and Engagement during Visually Guided Behavior. Cell Rep. 33, (2020).

65. Prusky, G. T., Alam, N. M., Beekman, S. & Douglas, R. M. Rapid Quantification of Adult and Developing Mouse Spatial Vision Using a Virtual Optomotor System. Invest. Ophthalmol. Vis. Sci. 45, 4611–4616 (2004).

66. Reward Modulates Visual Responses in the Superficial Superior Colliculus of Mice | Journal of Neuroscience. https://www.jneurosci.org/content/43/50/8663.

67. Burgess, C. P. et al. High-Yield Methods for Accurate Two-Alternative Visual Psychophysics in Head-Fixed Mice. Cell Rep. 20, 2513–2524 (2017).

68. Meshulam, L. et al. A brain-wide map of neural activity during complex behaviour. Nature 645, 177–191 (2025).

69. Marshel, J. H., Garrett, M. E., Nauhaus, I. & Callaway, E. M. Functional Specialization of Seven Mouse Visual Cortical Areas. Neuron 72, 1040–1054 (2011).

70. Han, X., Vermaercke, B. & Bonin, V. Diversity of spatiotemporal coding reveals specialized visual processing streams in the mouse cortex. Nat. Commun. 13, 3249 (2022).

71. Parker, P. Neural coding and circuitry of active vision in mice. J. Vis. 25, 1604–1604 (2025).

72. Judák, L. et al. Moculus: an immersive virtual reality system for mice incorporating stereo vision. Nat. Methods 22, 386–398 (2025).

73. Isaacson, M. et al. MouseGoggles: an immersive virtual reality headset for mouse neuroscience and behavior. Nat. Methods 22, 380–385 (2025).

74. Hunt, J. B. et al. Diverse and dynamic influences of saccades on visual representations in the mouse superior colliculus. Proc. Natl. Acad. Sci. 122, e2425788122 (2025).

75. Millman, D. J. et al. VIP interneurons in mouse primary visual cortex selectively enhance responses to weak but specific stimuli. eLife 9, e55130 (2020).

76. Prins, N. The psychometric function: The lapse rate revisited. J. Vis. 12, (2012).

77. Gupta, D., DePasquale, B., Kopec, C. D. & Brody, C. D. Trial-history biases in evidence accumulation can give rise to apparent lapses in decision-making. Nat. Commun. 15, 662 (2024).

78. Birman, D. et al. Interactive data exploration websites for large-scale electrophysiology. 2024.06.07.597950 Preprint at https://doi.org/10.1101/2024.06.07.597950 (2024).